Ecological Informatics 46 (2018) 166–178

Contents lists available at ScienceDirect

Ecological Informatics

journal homepage: www.elsevier.com/locate/ecolinf

# Evaluation of hydrologic and meteorological impacts on dengue fever incidences in southern Taiwan using time-frequency analysis methods

Christina W. Tsai*, Ting-Gu Yeh, You-Ren Hsiao

*Department of Civil Engineering, National Taiwan University, Taipei, Taiwan, ROC*

ARTICLE INFO

*Keywords:*
Climate change
Dengue fever
Time-frequency analysis
Hilbert Huang transform
Wavelet transform
Cross correlation

ABSTRACT

Extreme weather events are occurring more frequently as a result of climate change. Recently dengue fever has become a serious issue in southern Taiwan. It may have characteristic temporal scales that can be identified. Some researchers have hypothesized that dengue fever incidences are related to climate change. This study applies time-frequency analysis to time series data concerning dengue fever and hydrologic and meteorological variables. Results of two time-frequency analytical methods - the Hilbert Huang transform (HHT) and the Wavelet Transform (WT) are compared and discussed. As a result, a more effective time-frequency analysis method will be identified to analyze relevant time series data. The most influential time scales of hydrologic and meteorological variables that are associated with dengue fever are determined. Finally, the linkage between hydrologic/meteorological factors and dengue fever incidences can be established using time-dependent intrinsic correlation (TDIC) approaches.

## 1. Introduction

In recent years, dengue fever has become a significant public health issue in southern Taiwan. Extensive research in epidemiology and public health has suggested that large dengue fever outbreaks are strongly associated with hydrologic events. Additionally, climate change significantly increases the frequencies of both extreme dengue fever events and extreme hydrologic events. The Zika virus (ZIKV), which is spread by daytime-active Aedes mosquitoes, has recently had a severe impact in Brazil. Mosquito borne diseases have gained significant awareness due to their threat to human health. More researchers (Chao et al., 2014; Chen et al., 2010a, 2010b; Chen and Hsieh, 2012; Li et al., 2016; Liao et al., 2014; Tseng et al., 2009; Tung et al., 2014; Wu et al., 2009; Yu et al., 2011) are paying attention to the dengue fever disaster in Taiwan.

Statistical models for analyzing the correlation between outbreaks of the dengue fever and some weather-related variables such as precipitation, temperature and relative humidity have been proposed. Benjamin (2011) utilized search query surveillance to develop a predictive system, and compared three models for predicting the number of incidences of dengue fever. Chien and Yu (2014) used the distributed lag nonlinear model (DLNM), which considers delayed effects and nonlinear effects of meteorological factors on the spatiotemporal patterns of dengue fever incidences, to estimate the risk of dengue fever given various weather variables (Chien and Yu, 2014). Chiu et al. (2014) quantified the risk of dengue fever using a threshold-based quantile regression method, which can account for the spatial characteristics of dengue fever (Chiu et al., 2014).

The studies that are cited above all used time series weather data to investigate the correlation of weather variables with dengue fever. However, the utilized data are embedded with multiple time scales, which include daily, weekly, and seasonal, among others. For example, precipitation time series data may result from rainfall events of various time scales, such as typhoons and the East Asian heavy precipitations. In this sense, the statistical models in prior studies cannot extract multiple time scales from time series data.

Dengue fever events are speculated to be related to extreme hydrologic events. This study thus uses time-frequency analysis to extract extreme events from original data, and discusses the relationships between incidences of dengue fever and hydrologic events on different time scales. Moreover, the hydrologic events that importantly affect incidences of dengue fever will be identified.

In particular, this investigation will elucidate the correlation between incidences of dengue fever and hydrologic factors, including precipitation, temperature, relative humidity and El Niño events, which are associated with different time scales, using time frequency analysis. Numerous time-frequency analysis methods have been proposed in the last decade. In this study, two of the most well-known time-frequency analysis methods are compared.

Time-frequency analysis is an improvement upon the Fourier

* Corresponding author.
*E-mail address:* cwstsai@ntu.edu.tw (C.W. Tsai).

https://doi.org/10.1016/j.ecoinf.2018.05.002
Received 10 October 2017; Received in revised form 8 March 2018; Accepted 21 May 2018
Available online 22 May 2018
1574-9541/ 

**Table 1**
Comparison of time-frequency methods.

| Method | Window function | Non-stationary | Non-linear | Shortcoming |
|---|---|---|---|---|
| Fourier transform | yes | no | no | only for stationary |
| Short time Fourier transform (Heisenberg, 1927) | yes | yes | no | fixed window length |
| Wigner distribution function (Wigner, 1932) | no | yes | no | cross turn problem |
| Continuous Wavelet transform | yes | yes | no | only for linear system |
| Hilbert-Huang Transform (Huang et al., 1998) | no | yes | yes | weak mathematical properties |

transform (Aceros Moreno et al., 2004; Balocchi et al., 2004; Daubechies, 1990; Fukushima et al., 2014; Han et al., 2013; Park and Roesner, 2012; Schuchardt and Siesler, 2016; Stankovic et al., 2003; Suen et al., 2015; Zhang et al., 2016). The Fourier transform is usually the first method of frequency analysis (Eq. (1)) that comes to mind. It has contributed hugely to many fields (Cao and Lu, 2015; Daubechies, 1990; Gabor, 1946; Huang et al., 1998; Liu, 2015; Mansour and Sahar, 2000; Mesfioui et al., 2012; Reuben et al., 2014; Suriyawichitseranee et al., 2015; Torrence and Compo, 1998; Yang et al., 2010). However, the Fourier transform has limitations because it uses a time integral from negative infinity to positive infinity. This operation loses information from the time domain so the method cannot be used to analyze "unsteady" data involving frequencies that change over time. Therefore, the Fourier transform cannot be applied to obtain an instantaneous frequency.

$$X(\omega) = \int_{-\infty}^{\infty} x(t)e^{-j\omega t}dt,\ \omega \in (-\infty,\infty) \tag{1}$$

Researchers thereby developed time-frequency analysis (Eq. (2)) to analyze unsteady signals. The short-time Fourier transform (STFT) is a method of time-frequency analysis that is an improvement upon the Fourier transform, based on a very simple concept (Arabaci and Bilgin, 2007; Liu et al., 2015; Okumura, 2011). The short-time Fourier transform uses a window function to cut the signal into several segments, and the Fourier transform is then applied to each segment.

$$X(t,\omega) = \int_{-\infty}^{\infty} w(t-\tau)x(\tau)e^{-j\omega\tau}d\tau \tag{2}$$

Although the short-time Fourier transform can be used to analyze an unsteady signal, it also has some limitations. It does not yield high-resolution results along the time axis and the frequency axis simultaneously (Heisenberg, 1927). Furthermore, computational efficiency was a major issue in time-frequency analysis in the 20th century owing to limitations on computing capacity. Many modified short-time Fourier transforms, such as the spectrogram, the asymmetric STFT and the S transform, were developed to enhance computational efficiency.

Wigner (1932) proposed the Wigner distribution function (WDF) for obtaining high-resolution results in the time-frequency domain as shown in Eq. (3). The Wigner distribution function still suffers from cross turn and cannot be used to analyze complicated signals. Additionally, the Wigner distribution function is more computationally demanding than the short-time Fourier transform.

$$W(t,\omega) = \int_{-\infty}^{\infty} x(t+\tau/2)\cdot x^{*}(t-\tau/2)e^{-j\omega\tau}d\tau \tag{3}$$

Modifications of the Wigner distribution function include Cohen's Class Distribution, the Pseudo L-Wigner Distribution and the Gabor-Wigner Transform (Cho et al., 2010; Deprem and Cetin, 2015; Hory et al., 2001; Hu et al., 2015; Jing and Jiegang, 2009; O'Neill and Williams, 1998; Xu et al., 2016). Yen (1994) extended the method by defining wave packets that reduce a complex data set to a finite number of simple components and using the Wigner distribution function (Yen, 1994). Unfortunately, Yen's method suffers from poor computational efficiency.

The wavelet transform is another well-known time-frequency method, which was first utilized in seismology (Daubechies, 1990). The advantages of the wavelet transform are its varying time-frequency resolution and multiple scale zooming. Therefore, the wavelet transform is more effective than the STFT for analyzing low-frequency scale signals.

The above time-frequency analysis methods are all based on the Fourier transform, and the use of basis functions to capture the original data. They cannot be used to analyze nonlinear systems. The Hilbert transform is used to obtain instantaneous frequencies, overcoming the difficulty associated with the Fourier transform (Andrade et al., 2004; Bieda et al., 2015; Diaz and Esteller, 2007; Hanus, 2015; Huang et al., 1998; Valtierra-Rodriguez et al., 2013; Wu et al., 2016).

Although the Hilbert transform can directly yield instantaneous frequencies, it has shortcomings. It can only be used to analyze a sinusoid-like signals, which are those with properties of sine and cosine waves. Huang et al. (1998) presented empirical mode decomposition (EMD) (Huang et al., 1998). This method can be used to decompose a signal into various components, which have the properties of sinusoid-like signals. Huang called these components "intrinsic mode functions" (IMFs). Empirical mode decomposition (EMD) overcomes the shortcoming of the Hilbert transform. The Hilbert Huang transform (HHT) involves both empirical mode decomposition (EMD) and the Hilbert transform (HT) (Rao and Hsu, 2008).

Another advantage of HHT is its use of IMFs rather than particular basis functions, which are commonly used in other time-frequency analysis methods, to analyze signals. The IMFs retain the properties of the original data so HHT is more useful than other time-frequency methods for analyzing non-linear systems. Recently, time-frequency analysis methods have attracted more attention, as computational efficiency has significantly increased. Table 1 summarizes the above comparisons of time-frequency methods.

Time-frequency analysis methods can be applied to nonlinear and non-stationary signals. Most time series data are obtained from the natural world as nonlinear and non-stationary signals. Information or trends can be identified by decomposing or expanding the original time series data. In this work, several meteorological and hydrologic factors related to dengue fever are considered.

## 2. Methodology

### 2.1. Wavelet transform (WT)

The wavelet transform is extensively utilized in signal processing and image compression (Daubechies, 1990; Endo et al., 1998; Maria de Medeiros et al., 2005; Rabinovitch and Venetsanopoulos, 1997; Skublewska-Paszkowska and Smolka, 2008). It uses a mother wavelet function, which can be dilated, as a basis function. Since the window length of mother wavelet functions is dynamic, it changes with frequency. The formula for the wavelet transform is as follows.

$$WT(a,b) = \langle f(t), \psi_{a,b}(t)\rangle = \frac{1}{\sqrt{|a|}}\int_{-\infty}^{\infty} f(t)\psi^{*}\left(\frac{t-b}{a}\right)dt \tag{4}$$

where $a$ is the wavelet scale parameter; $b$ is the wavelet translation parameter; $\Psi$ is the wavelet mother function; $\Psi^{*}$ is the complex conjugate of the wavelet mother function.

The wavelet transform resolves the issue that the window in the short-time Fourier transform is too short for analyzing low-frequency

data. Time-frequency analysis is therefore more useful than conventional methods in data analysis. The wavelet transform does not use a window function but a wavelet mother function. Numerous mother wavelet functions have recently been presented such as the Harr wavelet, the Morlet wavelet, and the Mexican hat wavelet (Haar, 1910; Meyer, 1991; Morlet et al., 1982). The scale parameter $a$ dilates the mother wavelet function. The scale parameter $b$ translates the mother wavelet function.

In this study, the Morlet mother wavelet function widely used in data analysis, is chosen as the basis function (Liu et al., 2016; Morlet et al., 1982; Wei and Feng, 2015). It is expressed as follows.

$$\psi(x) = e^{-x^2}\cos\left(\pi\sqrt{\frac{2}{ln\,2}}x\right) \tag{5}$$

### 2.2. Hilbert-Huang Transform (HHT)

Huang et al. (1998) developed the Hilbert-Huang Transform (HHT), which consists of two parts - empirical mode decomposition (EMD) and Hilbert spectral analysis (HSA) (Huang et al., 1998).

#### 2.2.1. Hilbert spectral analysis (HSA)

The Hilbert transform can be used to obtain the instantaneous frequency of sinusoid-like time series data (Boche and Monich, 2012; Chaudhury and Unser, 2011; Huang et al., 1998; Hudspeth and Medina, 1988). It is expressed as

$$Y(t) = \frac{1}{\pi}P\int_{-\infty}^{\infty}\frac{X(t')}{t-t'}dt' \tag{6}$$

where $P$ is the Cauchy principal value. The Hilbert transform exists for all functions of class $L^p$ (Titchmarsh, 1948). Furthermore, combining $X(t)$ with $Y(t)$ could yield an analytic signal,

$$Z(t) = X(t) + \mathrm{i}Y(t) = a(t)e^{i\theta(t)} \tag{7}$$

in which

$$a(t) = [X^2(t) + Y^2(t)]^{1/2},\ \theta(t) = \arctan\left(\frac{Y(t)}{X(t)}\right) \tag{8}$$

where $a$ is the amplitude of the signal, and $\theta$ denotes the phase of the signal.

Applying the Hilbert transform to non-sinusoid-like time series data may result in error. Huang et al. (1998) presented several well-known signals as examples, and showed that the Hilbert transform yields errors (Huang et al., 1998). To solve this problem, they proposed Empirical Mode Decomposition.

#### 2.2.2. Empirical Mode Decomposition (EMD)

Empirical Mode Decomposition is a method for decomposing nonlinear and nonstationary data into several intrinsic mode functions (Barner and Weng, 2008; Du and He, 2009; Song et al., 2007; Wu and Huang, 2009; Wu and Huang, 2010; Oberlin et al., 2012). To satisfy the definitions of the intrinsic mode function, envelopes that are defined in terms of local maxima and minima are separately utilized to decompose original data.

First the extreme point is identified, and all local maxima are connected by a cubic spline line to form the upper envelope. Second, the same process is applied to local minima to generate the lower envelope. All of the original data should be between the upper and the lower envelopes. The mean of the upper and lower envelopes is denoted as $m_1$. The difference between the original data and $m_1$ $m_1$is the first component, $h_1$

$$x(t) - m_i = h_i \tag{9}$$

The process is iterated until the criterion of IMF definition is met. After all of the IMFs, $c_j$, are extracted, the residual, $r_n$, component is regarded as the trend of the original signal $x(t)$, i.e.,

$$x(t) = \sum_{j=1}^{n} c_j + r_n \tag{10}$$

Compared to the Fourier based algorithm, e.g., short time Fourier transform and wavelet transform, the EMD algorithm does not make an assumption of the basis function a priori. Consequently, this process has the adaptive property, which can be used to execute nonlinear and nonstationary signal filtering without generating spurious harmonics (Huang et al., 1998; Flandrin and Gonçalvès, 2004; Huang and Schmitt, 2014).

#### 2.2.3. Intrinsic mode functions (IMFs)

Each component of data that is obtained by decomposition from the original data is constrained by the Hilbert transform. Huang et al. (1998) presented the intrinsic mode function (Huang et al., 1998), which satisfies the following two conditions; (1) the number of extreme points and the number of zero crossings must equal to or differ by one, and (2) at any point, the mean value of the envelope defined by the local maxima or minima is zero. The mean value of the intrinsic mode function is zero, based on its first definition. The second definition of the function prevents the instantaneous frequency from exhibiting fluctuations that do not cross zero, induced by asymmetric wave forms. Such an intrinsic mode function supports analysis using the Hilbert transform.

### 2.3. Estimation of intrinsic correlation

The cross-correlation coefficient (Pearson correlation) is often used to measure the relationship between two signals. However, under the stationary and linear assumption of the cross-correlation coefficient, one might obtain unphysical correlations when the signals are mixture of multiscales, noises, phase shifts, frequency shifts or trends. Therefore, a nonlinear, nonstationary, and multiscale framework of correlation estimation is desirable. To decrease the distortion resulting from data nonstationarity, Papadimitriou et al. (2006) measured the cross correlation with sliding windows. It should be noted that the technique may provide unphysical correlation without proper selection of window length. Chen et al. (2010a, 2010b) presented a scale- and time-dependent correlation approach combining both the sliding window and the EMD algorithm to obtain time-dependent intrinsic correlation (TDIC). In this approach, EMD is used to extract the original signal into several scales, and the instantaneous frequency measurement is then utilized to select the adaptive window length in each scale. The TDIC of each pair of IMFs is defined as follows:

$$R_j(t_k^n) = Corr\left[c_{1j}(t_k^n), c_{2j}(t_k^n)\right] \text{ at any } t_k \tag{11}$$

where $Corr$ is the cross correlation coefficient of two signals and the sliding window. ${t_k}^n$ is

$$t_k^n = [t_k - nT_d/2, t_k + nT_d/2] \tag{12}$$

where the minimum sliding window length is selected to be $T_d = \max(T_{1j}(t_k), T_{2j}(t_k))$ where $T_{1j}(t_k)$ and $T_{2j}(t_k)$ are the instantaneous period of two signals. $n$ is any positive real number.

In addition to the TDIC approach, one is able to analyze the lag effect between two signals by applying the time-dependent intrinsic cross correlation (TDICC) approach, which is defined as

$$R_j(t_k^n, \tau) = Corr\left[c_{1j}(t_{w,\tau}^n), c_{2j}(t_{w,\tau}^n)\right] \text{ at any } t_k \tag{13}$$

where $t_{w,\tau}^{\ n} = [t_k - \tau - nT_d/2, t_k - \tau + nT_d/2]$ and $\tau$ represents the time lag.

## 3. Background (description of study area and data sets)

### 3.1. Dengue fever

The Dengue fever is caused by the dengue virus (DENV), which is spread by mosquitoes. It typically breaks out in the Central and tropical South America, South and Southeast Asia and many parts of tropical Africa. Dengue fever is a public health problem in southern Taiwan.

Aedes mosquitoes are the most common carrier of dengue fever. Aedes mosquitoes can generally be found between latitudes of 35° north and 35° south. The lifetime of the Aedes mosquitoes is close to a month. Meteorological and hydrologic factors such as temperature, precipitation and relative humidity play a vital role in the survival and distribution of Aedes mosquitoes, and hence influence the capacity of DENV transmission. The most comfortable temperature for Aedes mosquitoes is between 20 °C and 30 °C (Ebi and Nealon, 2016).

The symptoms of dengue fever are similar to those of the common cold and gastroenteritis, but some serious cases of dengue fever may be fatal. Those serious cases are normally dengue hemorrhagic fever, which is caused by secondary infections. Symptoms of dengue hemorrhagic fever are persistent high fever, rash and shock. Chien and Yu (2014) indicated the risk of dengue fever incidences in Taiwan is highly correlated to population and socioeconomic status. Fig. 1 reveals that the spatial distribution of dengue fever is very close to the spatial distribution of the population.

Fig. 2 plots the correlation between the incidences of dengue fever and the density of population. The former is proportional to the latter, but this positive correlation is nonlinear (correlation coefficient:ρ = 0.4576).

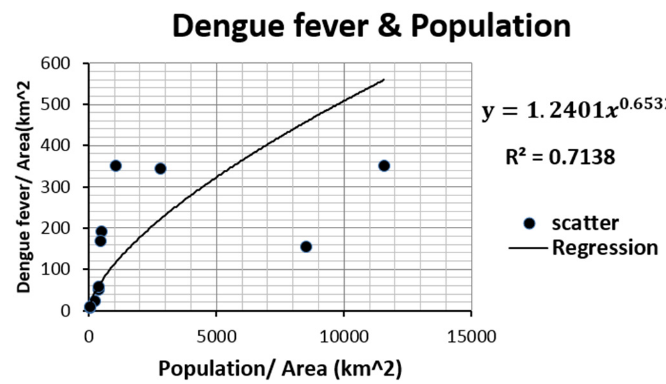


**Fig. 2.** Correlation between dengue fever incidences and population (correlation coefficient: ρ = 0.457624).

The main purpose of this paper is to investigate the temporal influence of meteorological and hydrologic factors on dengue incidences. The above spatial analysis results are intended for determining potential hotspots for data collection, thus avoiding the spatial factors to affect the result of time-frequency analysis.

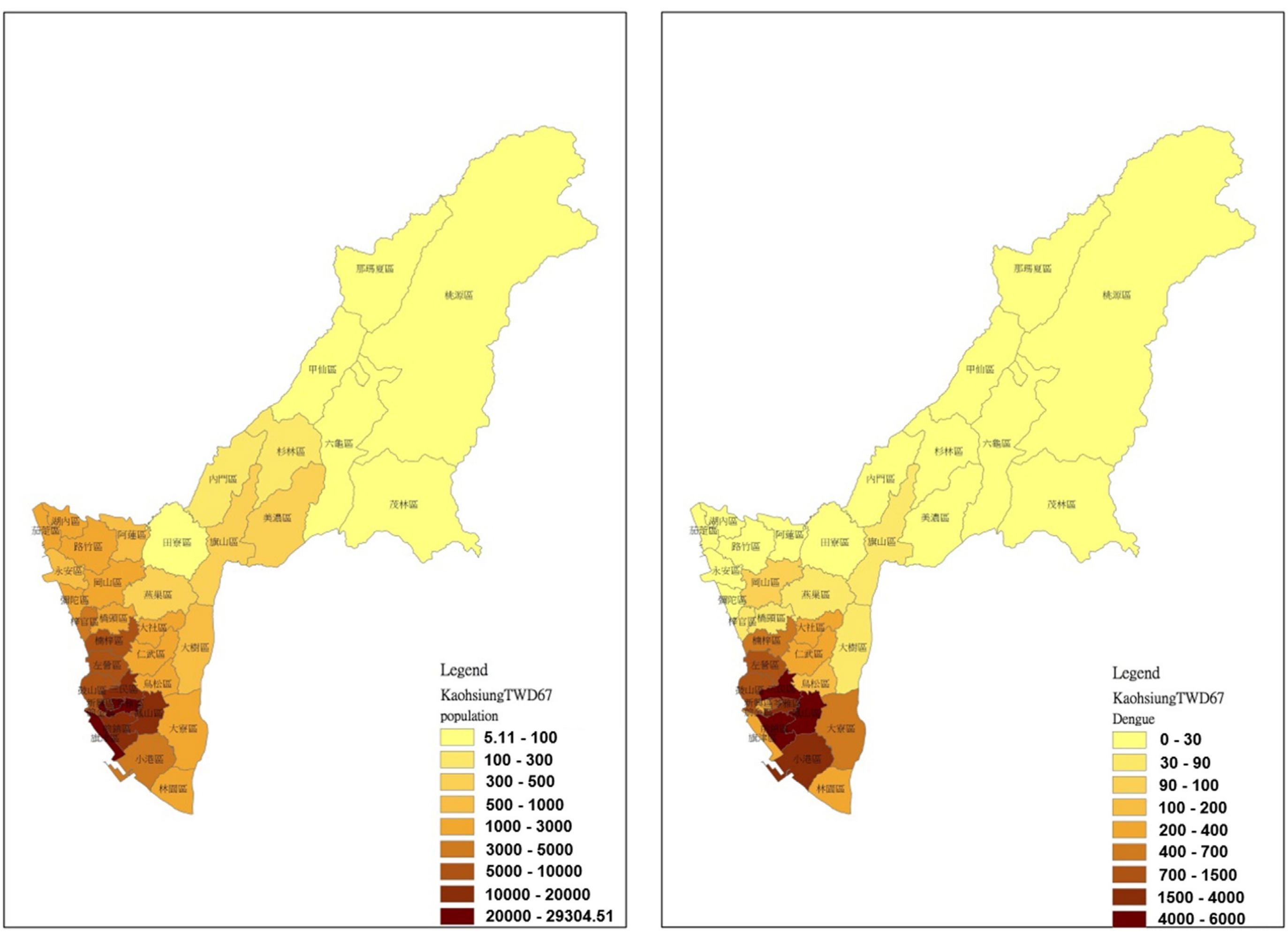


**Fig. 1.** Population (Left figure) and spatial distribution (Right figure) of dengue fever in Kaohsiung.

**Table 2**
Hydrologic variables in time-frequency analysis.

| Factor | Source | Region | Sampling time | Resolution |
|---|---|---|---|---|
| Number of dengue fever | Center for Disease Control | Kaohsiung | 2000–2015 | Week |
| Precipitation | Central Weather Bureau | Kaohsiung (QianZhen) | 2000–2015 | Day |
| Temperature | Central Weather Bureau | Kaohsiung | 2000–2015 | Day |
| Humidity | Central Weather Bureau | Kaohsiung | 2000–2015 | Day |
| Southern Oscillation Index (SOI) | The Australian Government Bureau of Meteorology | Tropical Pacific | 2000–2015 | Month |
| Oceanic Niño Index (ONI) | NOAA National Weather Service Climate Prediction Center | The Niño 3.4 region (5°N-5°S, 120°–170°W) | 2000–2015 | Month |

### *3.2. Study area and data collection*

Kaohsiung is the third largest city in Taiwan with a population of approximately 2.77 million people. The area of this region is 2951.85 $km^2$. During 2014 and 2015, the dengue fever hit southern Taiwan, and over 90% of the total number of the incidences of dengue fever occurred in this region. Kaohsiung was one of the centers of the incidences of dengue fever. In this study, the correlation between hydrologic time series data from 2000 to 2015 with incidences of dengue fever is analyzed. Data from 1/1/2016–12/31/2016 are included to reduce the boundary problem in the EMD algorithm so that the intended study period, year 2000–2015, can be more efficiently modeled. Dengue fever time series data are obtained from the Taiwan Central Weather Bureau (TCWB). Extreme climate results from El Niño-Southern Oscillation (ENSO) is thought to affect the outbreaks of vector-borne diseases (Ebi and Nealon, 2016; Van Panhuis et al., 2015). Accordingly, the Southern Oscillation Index (SOI) obtained from the Australian Government Bureau of Meteorology (BOM) and the Oceanic Niño Index (ONI) obtained from the National Oceanic and Atmospheric Administration (NOAA) and National Weather Service Climate Prediction Center are considered. Table 2 lists all of the hydrologic variables used in the time-frequency analysis herein.

## 4. Time-frequency analysis: results and discussion

### *4.1. Analysis of wavelet spectrum*

Fig. 3 presents the wavelet spectrum for incidences of dengue fever, showing the highest energy in the year of 2002, 2014 and 2015. The periodicity of outbreaks of dengue fever is 0.5 to 8 years. Dengue fever outbreaks are therefore events with multiple time scales, and the time scales are non-stationary.

Extreme dengue fever events are complex and have multiple time scales in 2002, 2014 and 2015. The energy density in the spectrum is the amplitude squared of the wavelet coefficients, and, in this case, is the number of dengue fever outbreaks. The three high-energy regions in Fig. 3(c) have significant time scales of one, two, and four to eight years, which indicate that dengue fever illness might be associated with some seasonal impact and multi-seasonal variation.

In the seasonal scale, precipitation, relative humidity and temperature are considered as the influential factors. Fig. 4 presents a wavelet spectrum of precipitation in Qianzhen, which is a hotspot of dengue fever in Kaohsiung. The characteristic time scale of one year is found to be associated with precipitation seasons in Taiwan. The precipitation seasons of Kaohsiung result from plum rain, monsoon rain and typhoons. Some discontinuous energy is observed with periods from 0.125 to 0.5 year. The period from 0.125 years to 0.25 years corresponds to four to eight occurrences in one year. These high-frequency events correspond to typhoons and afternoon thundershowers, which are typically experienced in the area.

Interestingly, comparing Figs. 3 and 4 reveals that dengue fever does not have high-frequency components. In Fig. 4(b), the energy of high-frequency incidences is concentrated from 2005 to 2010, and no extreme dengue fever incidences occurred in that period. Therefore, seasonal precipitation may be more strongly correlated with incidences of dengue fever than are typhoons and afternoon thundershowers (which are high-frequency events).

Temperature and relative humidity have only one significant frequency component, as displayed in Figs. 5 and 6, which corresponds to seasonal variation. This frequency is the same as that identified in the precipitation data, as expected. Precipitation strongly affects relative humidity. The energy of relative humidity is high from year 2014 to 2016 in Fig. 6 (b), indicating that the variation of relative humidity from 2014 to 2016 is very large. Arcari et al. (2007) similarly found

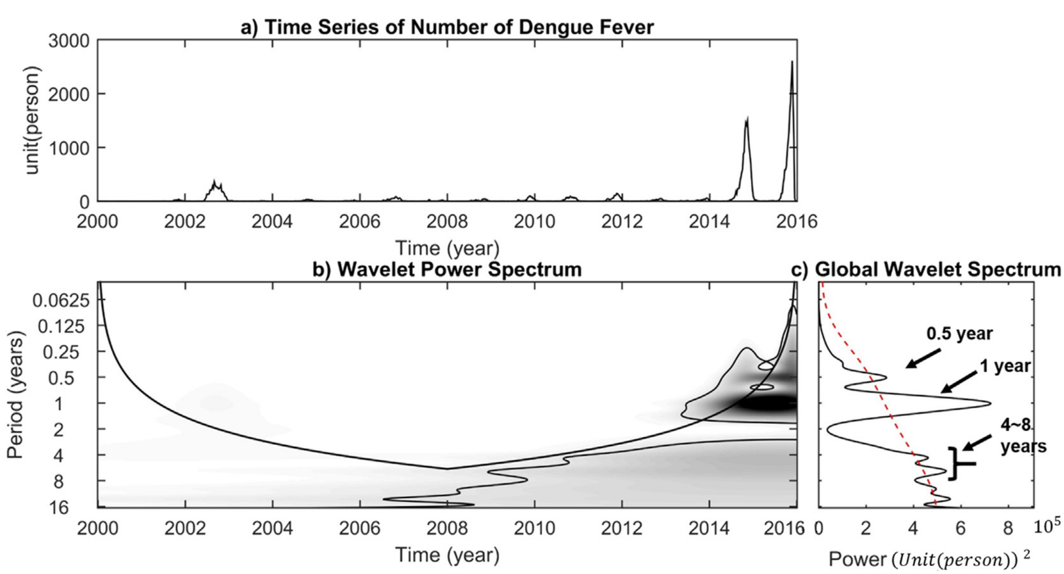


**Fig. 3.** Wavelet spectrum of dengue fever from 2000 to 2015.

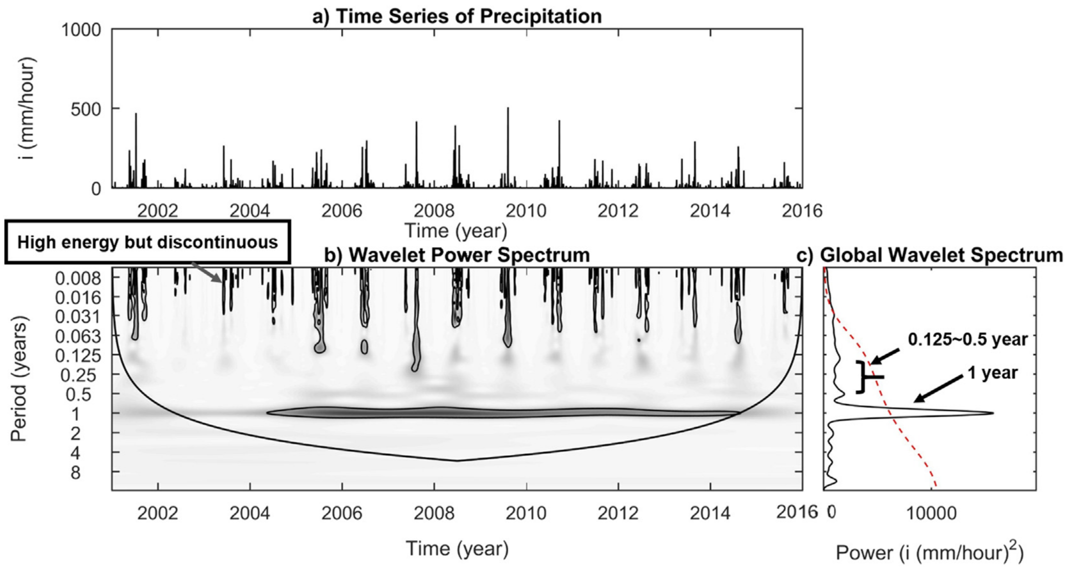


**Fig. 4.** Wavelet spectrum of precipitation in QianZhen, Kaohsiung, from 2000 to 2015.

that relative humidity is significantly correlated with outbreaks of dengue fever (Arcari et al., 2007).

In the scale corresponding to long-term climate change, the Southern Oscillation Index (SOI) and the Oceanic Niño Index (ONI) are selected as influential factors. The choice is based on the strong correlation between El Niño-Southern Oscillation (ENSO) and Dengue fever incidences in previous studies (Fisman et al., 2016; Kolivras, 2010; Van Panhuis et al., 2015). Fig. 7 shows the wavelet spectrum of SOI of El Niño events. Sustained negative values of SOI below −7 typically indicate El Niño episodes. Characteristic time scales of both 3–4 years and 8-years are observed in Fig. 7(b), while the latter scale is not in the cone of influence (COI) region, which is the region not affected by the edge effect. The same scales are also detected in Fig. 7(c) in a global sense.

The Oceanic Niño Index (ONI) is compared with the SOI. NOAA defines an El Niño incident when the ONI exceeds +0.5. Fig. 8 shows the characteristic time scales (3 to 4, and 8 to 9 years) of ONI, and these are similar to those of the SOI.

The wavelet transform is a powerful approach in analyzing temporal frequency distributions of nonstationary signals, however, the shortcoming of having non-adaptive nature makes it difficult to capture the nonlinear features. Moreover, the above drawback as well as the power leakage property make it hard to precisely quantify the temporal cross correlation. Compared to the wavelet spectrum, the Hilbert spectrum is able to provide sharper time-frequency distributions (Huang et al., 1998). On the other hand, it might be easier to locate the characteristic times scales in the wavelet spectrum. Hence, in this section, the wavelet spectrum is used to identify time scales of different hydrologic and meteorological time series data. In the following section, some IMFs that are obtained from various time series data will be identified according to their characteristic time scales. The temporal cross-correlation between variables will be discussed with reference to IMFs.

### 4.2. Hilbert-Huang Transform and temporal correlation analysis

In previous sections, seasonal and multi-seasonal relationships have been identified between Dengue fever incidences and the influential meteorological factors. Such quantitative association is then analyzed using TDIC and TDICC, based on the EMD algorithm and the selected

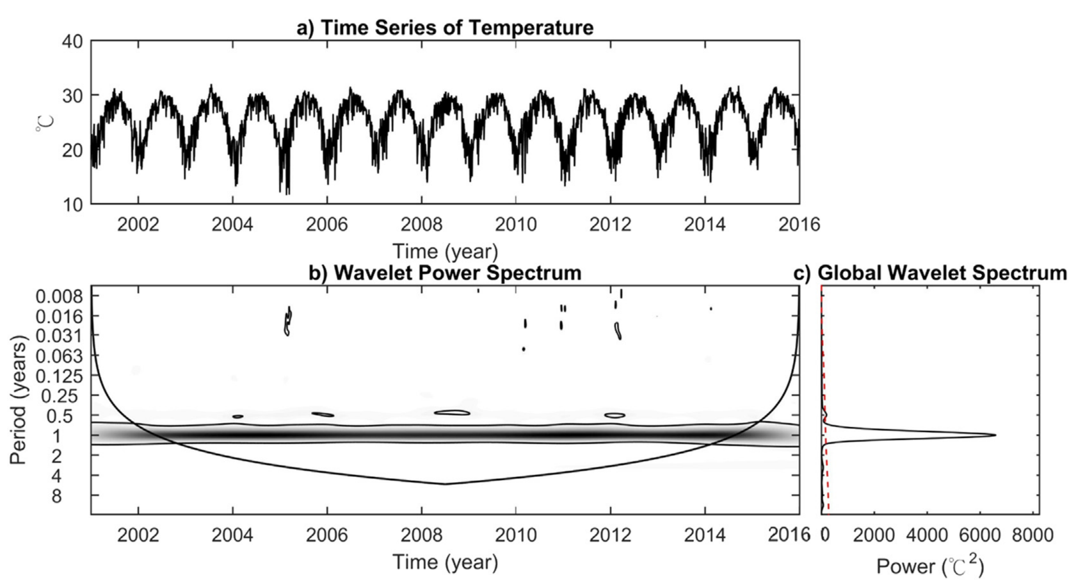


**Fig. 5.** Wavelet spectrum of temperature in Kaohsiung from 2000 to 2015.

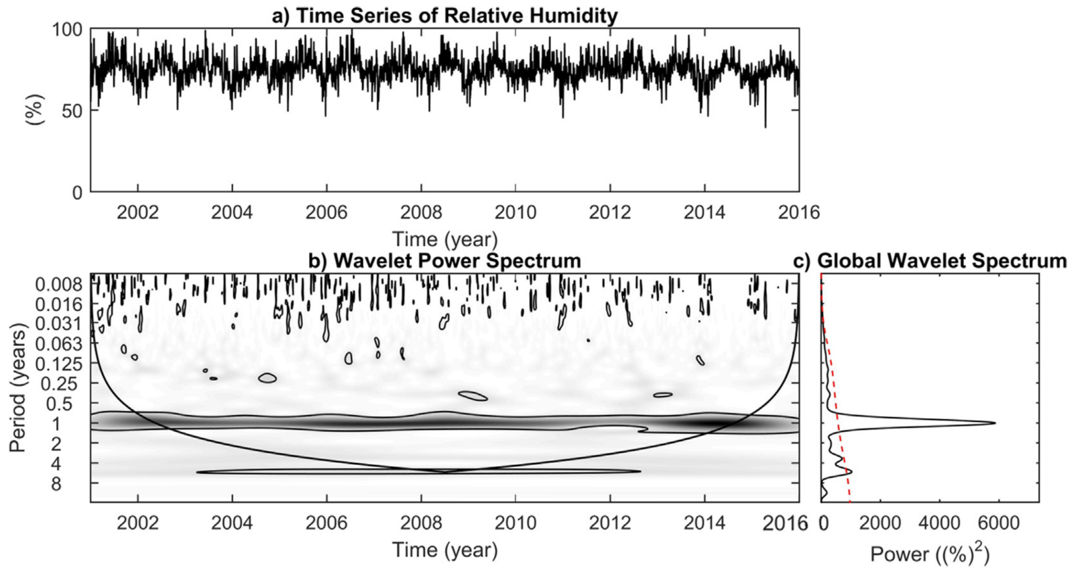


**Fig. 6.** Wavelet spectrum of relative humidity in Kaohsiung from 2000 to 2015.

sliding window, accordingly. The results are in contrast to the global cross-correlation with time lags from two aspects: the relationships between original signals and those between IMFs.

Fig. 9(a) delineates the decomposed modes of Dengue fever and precipitation at Qianzhen in the seasonal scale. Although Dengue fever and precipitation share similar characteristic time scales, outbreaks of dengue fever do not occur at precipitation peak times, indicating a potential temporal lag effect between two variables. Chien and Yu (2014) developed the distributed lag nonlinear model (DLNM) to describe the spatiotemporal influence of meteorological factors on Dengue fever incidences. The sensitive analysis performed to DLNM was used to determine the correlation between variables. A time lag of 8 to 15 weeks was observed between Dengue fever incidences and precipitation, as well as between Dengue fever incidences and temperature (Chien and Yu, 2014). Fig. 9(b) compares the cross correlation of IMFs with two original signals. With the original signals, the cross correlation without the time lag is 0.056; and the correlation for data with a 12-week lag is 0.222. On the other hand, with IMFs, the cross correlation without the time lag is 0.196 and the correlation for data with a 9-week lag is 0.347. Fig. 9(c) demonstrates the TDICC plot which describes the temporal fluctuation of cross correlation and the lag effect between IMFs. The plot reveals that localized correlations such as the white region (i.e., the temporal maximum positive correlated region) varies with time. However, in the global sense, the cross correlation has reduced to 0.347. Fig. 9 also shows that in endemic periods, such as 2002, 2014 and 2015, the lag is approximately 5–10 weeks, whereas for the remaining time period, the lag is around 8–18 weeks.

Fig. 10(b) compares the cross correlation of Dengue fever incidences with relative humidity. For the original signals, the cross correlation without the time lag is 0.241 with an ambiguous lag effect (i.e., the lag does not present any apparent peaks.). However, for IMFs, the cross correlation without the time lag is 0.196 and the correlation for data with a 12-week lag is 0.463. Fig. 10(c) depicts that in endemic periods, the lag is around 6–12 weeks, whereas for the remaining time period, the lag is approximately 8–21weeks.

The analogous phenomenon is observed in relation to temperature. Fig. 11(a) displays the decomposed modes of Dengue fever and temperature at Qianzhen in the seasonal scale. From Fig. 11(b), for the

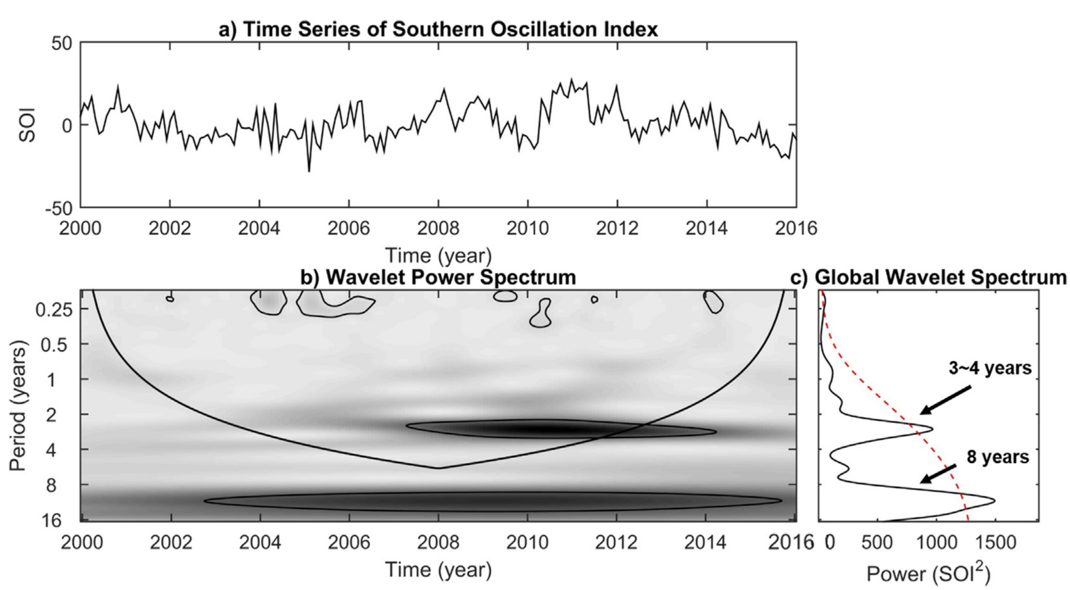


**Fig. 7.** Wavelet spectrum of Southern Oscillation Index (SOI).

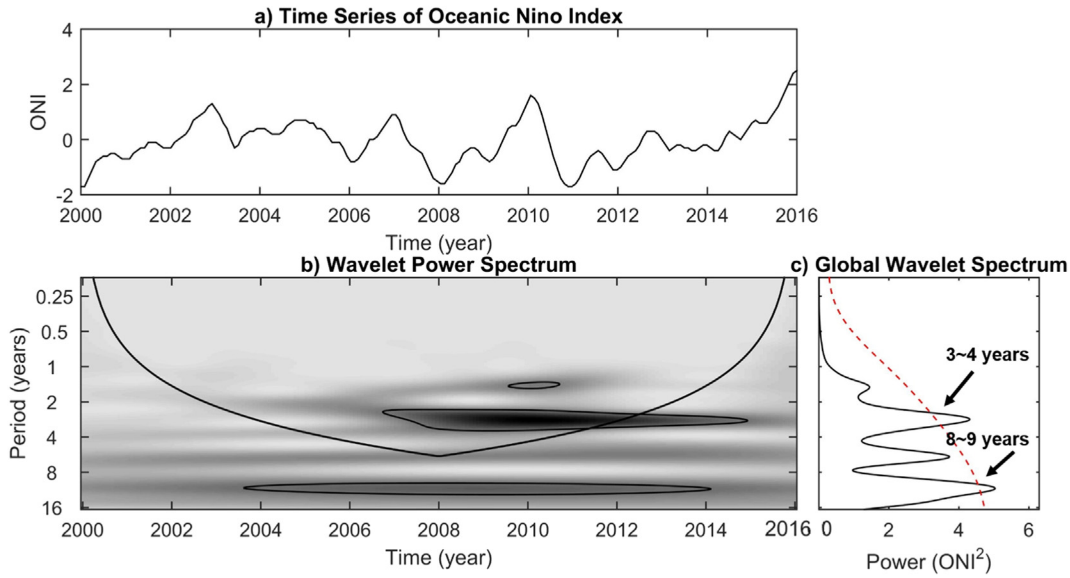


**Fig. 8.** Wavelet spectrum of Oceanic Niño Index (ONI).

original signals, the cross correlation without the time lag is 0.253, and the lag effect is also unclear. Conversely, for IMFs, the cross correlation without the time lag is 0.099 and the correlation for data with a 12-week lag is 0.418. Fig. 11(c) delineates that in endemic periods, the lag is around 5–10 weeks, whereas in normal time the lag is approximately 8–18 weeks. Fig. 12 displays a trend of increasing temperature of 1 °C from year 2000 to 2016, which reveals that at higher latitudes, it is more favorable for Aedes mosquitoes. Incidences of dengue fever appear to be moving northward (Kaohsiung in 2015; and Tainan in 2016).

Given the seasonality of dengue fever, the time scale of extreme events is of particular interest. In the preceding section, the time scale of multi-seasonal events was identified as four years, which is also the time scale of ENSO events. The IMFs of SOI and Dengue fever incidences with a time scale of close to four years is identified in Fig. 13(a). From Fig. 13(b), for original signals, the cross correlation without the time lag is −0.151, and the lag effect is unclear. On the opposite, for IMFs, the cross correlation without the time lag is −0.628 and the correlation for data with a 3-week lag is −0.647, which is not obvious. The negative correlation indicates that the outbreaks of Dengue fever are related to El Niño events.

Fig. 13(c) demonstrates the TDIC plot which describes the temporal fluctuation and identifies the period(s) of time with a particularly high cross correlation between IMFs with several choices of window length. It is noted that the peak of the triangular plot represents the global cross correlation, as the window selection is identical to the whole data length. In addition, since the minimum window selection is 4 year, the window center is from 2002 to 2014. In the TDIC plot, it is intriguing that the negative correlation is from the years before 2007 and after 2012, which are close to endemic periods. Nevertheless, two positive correlated eras are detected at around 2008–2009 and 2011–2012.

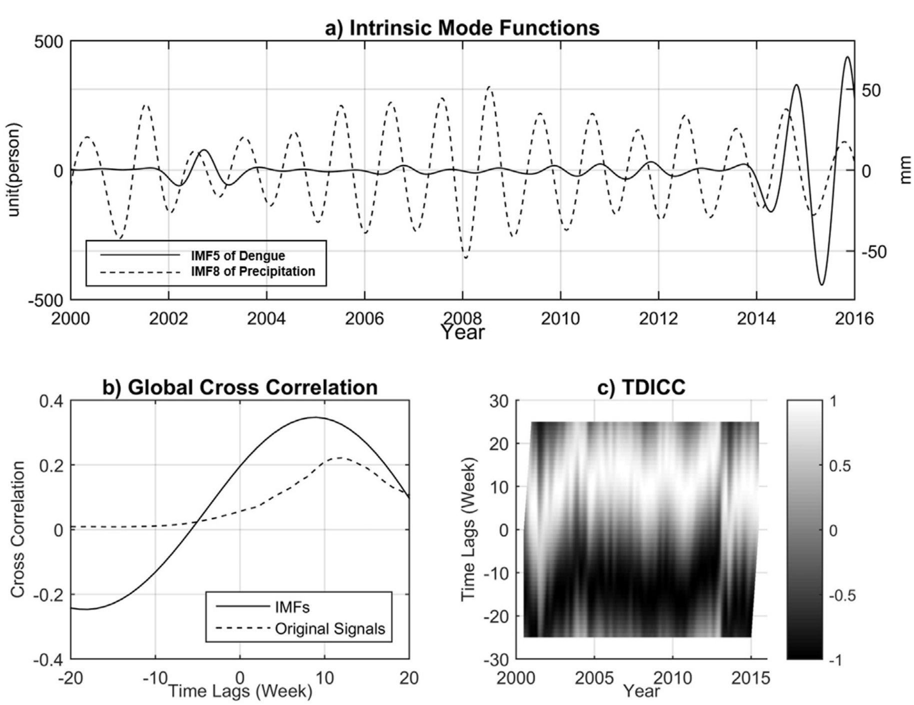


**Fig. 9.** (a) IMF5 of dengue fever and IMF8 of precipitation (QianZhen), (b) Global Cross Correlation, (c) TDICC (Window length: 52 weeks).

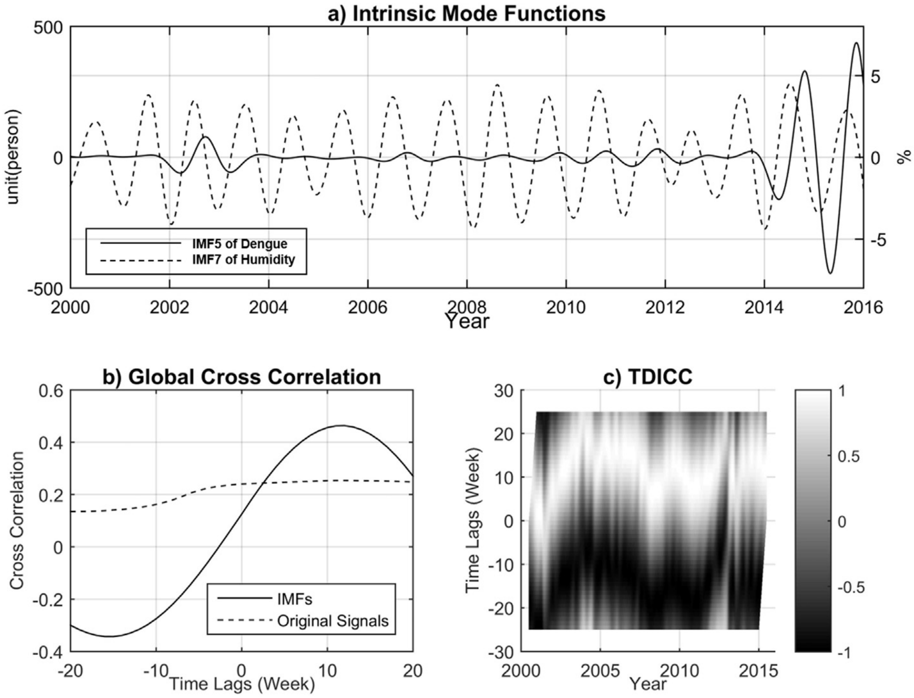


**Fig. 10.** (a) IMF5 of dengue fever and IMF7 of relative humidity, (b) Global Cross Correlation, (c) TDICC (Window length: 52 weeks).

These eras are found to be during La Niña events, reflecting that the La Niña events might have a slightly positive tendency with Dengue fever incidences.

The IMFs of ONI and Dengue fever incidences with a time scale of close to four years is identified in Fig. 14(a). From Fig. 14(b), the cross correlation without the time lag is 0.349 for original signals, and the cross correlation without the time lag is 0.734 for IMFs, indicating that Dengue fever events and El Niño events are proved to be highly associated. Both lag effects are not obvious for both the original signals and IMFs. In Fig. 14(c), the TDIC plot, compared with the TDIC of SOI, only shows a decreasing positive correlation with the detected La Niña events. The correlation of dengue fever incidences and ONI is positive in the whole study period.

The EMD, as a detrending approach, generates trends of each variable. Fig. 15(a) is a comparison between trends of Dengue fever incidences and SOI, indicating that occurrences of both dengue fever incidences and El Niño are increasing. The trend of ONI in Fig. 15(b) also supports the above findings.

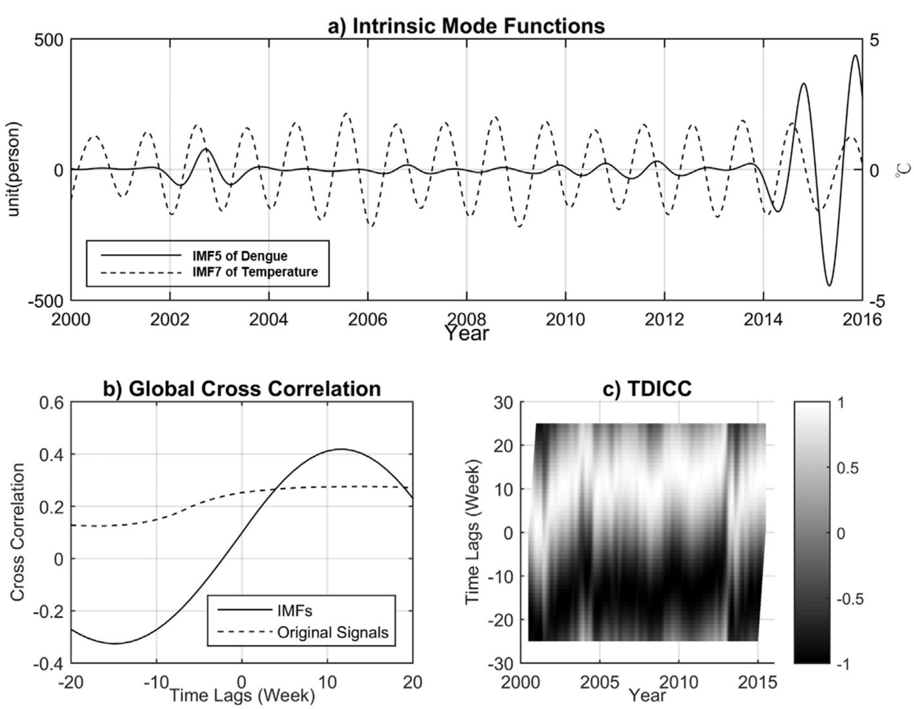


**Fig. 11.** (a) IMF5 of dengue fever and IMF7 of temperature, (b) Global Cross Correlation, (c) TDICC (Window length: 52 weeks).

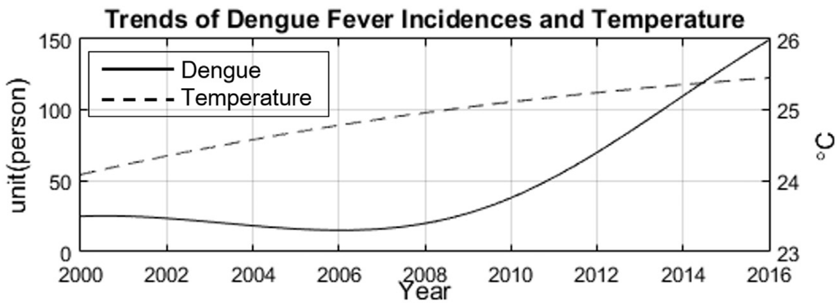


**Fig. 12.** Trend of Temperature in Kaohsiung.

## 5. Discussion

Over the past few decades, the mosquito borne diseases such as the dengue fever have become one of the most significant public health problems all around the world. Therefore, a better understanding of the mechanisms of Dengue fever incidences is critical to the control of epidemics. In the proposed study, the wavelet spectrum is performed to identify potential time scales in each variable.

A wavelet spectrum indicates the energy distribution of nonstationary and multiscale time series data in both the time domain and frequency domain. The length of the time series in this work is 16 years, so a time scale of 16 years or more cannot be regarded as having any physical meaning. Results from the wavelet spectrum delineate the characteristic seasonal scale (i.e., at the scale of regular events) and multi-seasonal scale (i.e., at the scale of extreme events) of Dengue fever incidences. Due to the non-adaptive nature of the wavelet spectrum discussed in the last paragraph of "Analysis of Wavelet Transform" section, further quantitative correlation measurements in relation to different hydrologic and meteorological time series data are identified from the EMD based TDIC and TDICC algorithms.

Regular seasonal dengue fever events are correlated with seasonal hydrologic and meteorological variations. In a global sense of correlation analysis, a time lag of 9–12 weeks is identified among IMFs in precipitation, relative humidity and temperature. The global time lag estimated by original signals, however, is unclear since the original signals are mixtures of complicated scales and noises. Such outcomes show a more reliable measurement by estimating lag effects on characteristic time scales.

In local sense of TDICC, Dengue fever events have a characteristic time lag of 8–18 weeks following the seasonal precipitation events in regular time during year 2000–2015, while the time lag is reduced to 5–10 weeks during the epidemic time. In the results of relative humidity, the regular time lag is 8–21weeks, whereas it turns out to be 6–12 weeks during the epidemic time. In the outcomes of temperature, the regular time lag is 8–18 weeks, whereas it turns out to be 5–10 weeks during epidemic time. Detection of a varying time lag effect in the seasonal scale is attributed to the nonlinear and localized properties of the proposed HHT framework. On the contrary, the Fourier-based methods might not always be applicable to investigating such effect since the basis function has been determined at the very beginning. The pre-determined basis function limits the investigation of nonlinear features of signals.

Intra-seasonal Dengue fever events in Taiwan are highly correlated with the occurrences of El Niño, from either the results of SOI or those of ONI. During the El Niño events, there is a tendency to have a warmer winter in Taiwan, and more precipitation in the following spring. The increasing temperature and precipitation may magnify the outbreaks of Dengue fever illness and result in the extreme dengue fever events.

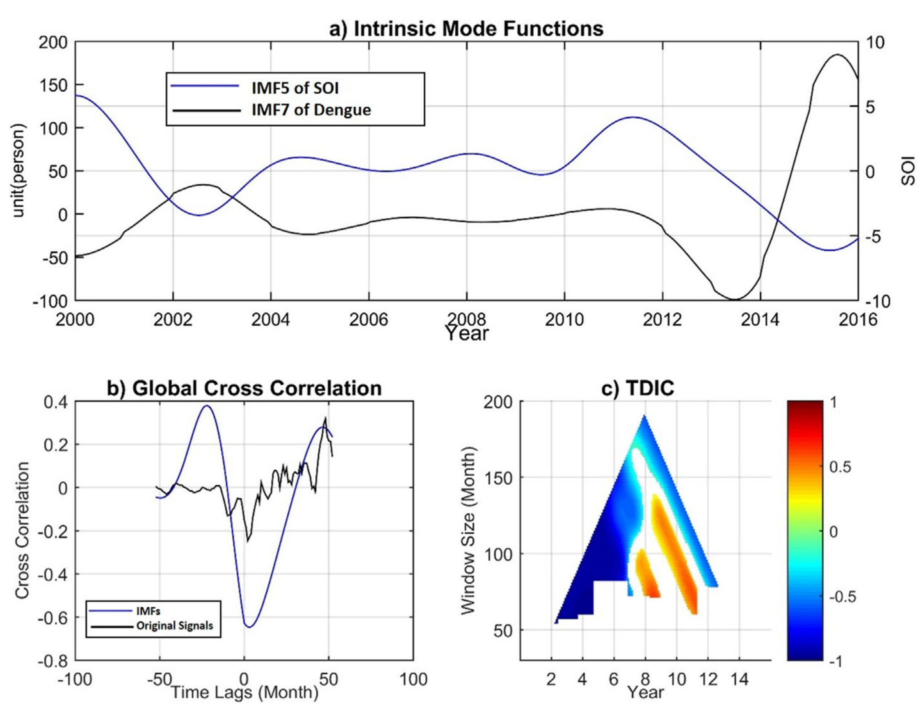


**Fig. 13.** (a) IMF5 of dengue fever and IMF5 of SOI, (b) Global Cross Correlation, (c) TDIC (The voids indicate the cross correlation is not significant at 5% significant level).

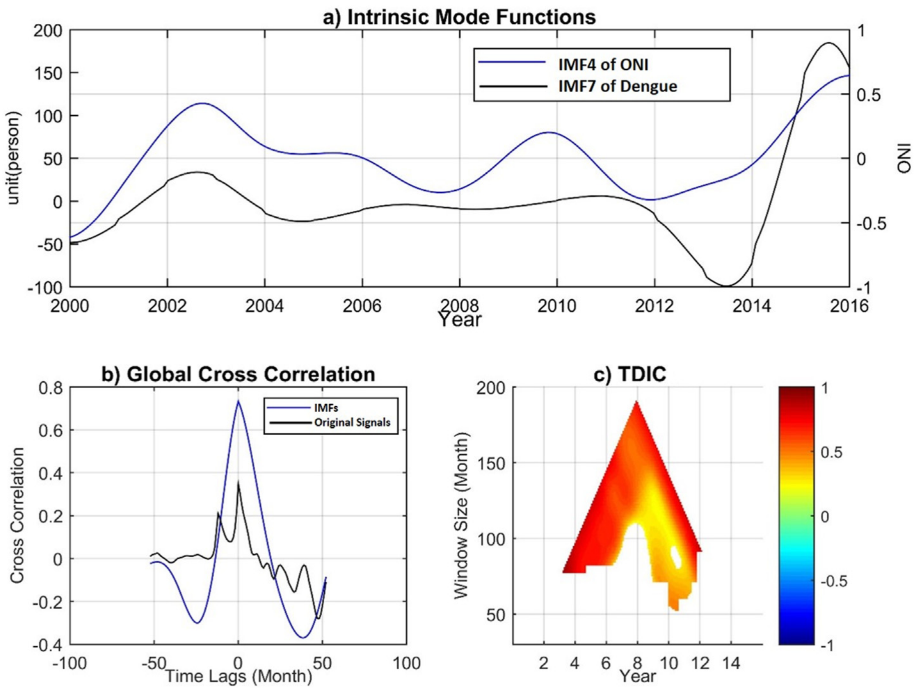


**Fig. 14.** (a) IMF5 of dengue fever and IMF5 of ONI, (b) Global Cross Correlation, (c) TDIC(The voids indicate the cross correlation is not significant at 5% significant level).

When compared in the seasonal scale, both SOI and ONI do not have an obvious lag effect with Dengue fever events. Finally, the results show some signs of climate change including trends of temperature and El Niño effects. With increasing temperature and El Niño intensity under long-term climate change, an increasing magnitude and intensity of Dengue fever incidences is observed. Long-term climate change is herein proved to be related to epidemic time of dengue fever outbreaks, and the result corresponding to the seasonal scale reveals the decreasing time lag effect. As such, one might conclude that the signal of El Niño events should be regarded as a wakeup call for government agencies to take urgent action in epidemic control.

Despite that the variation of lag effects between Dengue fever incidences and meteorological factors is detected with the TDICC plot in this study, meteorological factors, such as temperature, precipitation, relative humidity and evaporation, do not directly influence the outbreaks. For example, temperature may have a significant impact on all stages of the mosquito life cycle such as the biting rate, egg and immature mosquito development, development time of virus in the mosquito, and the survival rate (Christophers, 1960; Ebi and Nealon, 2016). Precipitation, relative humidity and evaporation influence the size, population, and behavior of Aedes mosquitoes. In addition, incidences of Dengue fever also vary with different water storage, land use, irrigation and population movement (Ebi and Nealon, 2016). Therefore, transmission of Dengue fever illness is a complicated process, which results in an uncertain lag effect. The corresponding studies are suggested to consider the uncertain lag effect in different scale in the

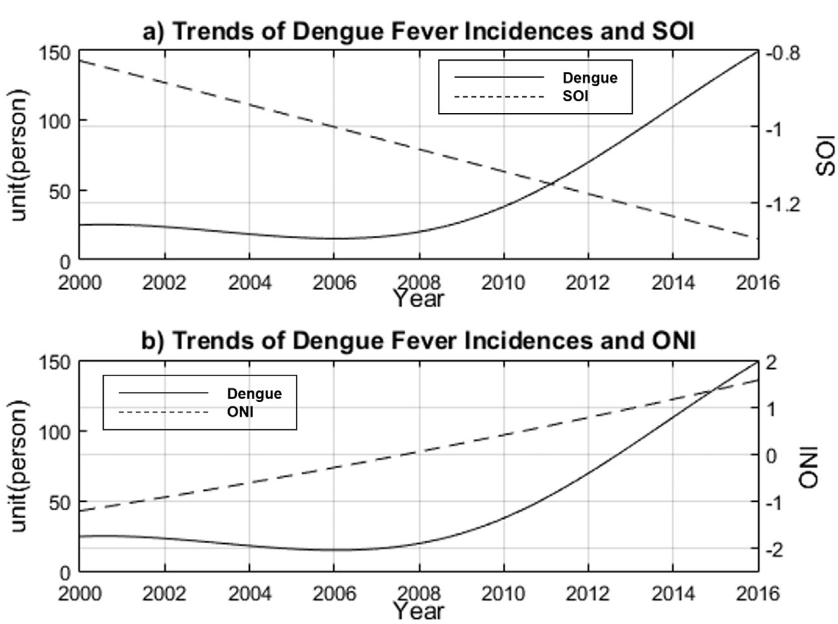


**Fig. 15.** (a) Trend of SOI (b) Trend of ONI.

nonlinear and nonstationary framework to gain more insights of this threatening vector-borne diseases in the future.

## 6. Conclusion

This study elucidates the correlation between dengue fever incidences and hydrologic/meteorological variables using various methods of time-frequency analysis (wavelet transform and HHT) and the moving correlation analysis (TDIC and TDICC). The dynamic length of the window in the wavelet transform can be used to accurately identify the critical components with different time scales in time series data. The HHT can decompose the original data into various IMFs without the assumption of basis functions. Extracting information from individual IMFs is easier than from original complex nonlinear and nonstationary events with multiple time scales.

The results herein demonstrate that the characteristic time scales of dengue fever incidences are one, four and eight years, respectively. Precipitation, relative humidity and temperature have the same annual time scale as dengue fever. The characteristic time lag of dengue fever incidences is identified to vary under different climate conditions. In a global sense of correlation analysis, a time lag of 9–12 weeks is identified. In the local sense, the TDICC plots indicate that the lag effects vary with time. The time lag would decrease during the epidemic time. The characteristic time scale of extreme dengue fever events (i.e., four years) is close to that of El Niño. Interestingly, the characteristic time scales of extreme dengue fever and El Niño are found to be similar. The frequency of both extreme dengue fever incidences and El Niño events is increasing.

The above results reveal that extreme dengue fever events are strongly correlated with El Niño events, such events are correlated to the decreasing lag effects of dengue fever and to the meteorological and hydrologic factors in the annual scale. Therefore, the Center for Disease Control should pay close attention to El Niño. Finally, we advise that precautions such us mosquito eradication should be taken in the middle of precipitation seasons to prevent dengue fever.

Although the impact of varying time lag characteristics of selected hydrologic and meteorological factors on dengue fever incidences has been detected based on the proposed time frequency analysis methods, the nonlinear influential factors on the Dengue fever incidences remain a complicated mechanism to be explored. Such mechanism is worth investigating in the future to improve the effectiveness of the epidemic control. It is also demonstrated that the EMD-based TDIC and TDICC algorithms are applicable to time series with multi-scales, nonlinear and nonstationary features.

## Acknowledgement

This research is supported by Taiwan Ministry of Science and Technology (MOST) under grant contract number 104-2628-E-002-011-MY3. Supplemental fund under grant number 105R7712 from National Taiwan University is also acknowledged 107L7708.

## References

Aceros Moreno, C.A., Sanchez, W.D., Rodriguez, D., 2004. The discrete chirp fourier transform and scale-frequency signal analysis. In: Proc., Proceedings of the IASTED International Conference on Circuits, Signals, and Systems, November 28–December 1. Acta Press, pp. 21–24.
Andrade, M.A., Messina, A.R., Rivera, C.A., Olguin, D., 2004. Identification of instantaneous attributes of torsional shaft signals using the Hilbert transform. IEEE Trans. Power Syst. 19 (3), 1422–1429.
Arabaci, H., Bilgin, O., 2007. The detection of rotor faults by using short time Fourier transform. In: Proc., 2007 IEEE 15th Signal Processing and Communications Applications, SIU, June 11–June 13. Inst. of Elec. and Elec. Eng. Computer Society, pp. 1–4.
Arcari, P., Tapper, N., Pfueller, S., 2007. Regional variability in relationships between climate and dengue/DHF in Indonesia. Singap. J. Trop. Geogr. 28 (3), 251–272.
Balocchi, R., Menicucci, D., Santarcangelo, E., Sebastiani, L., Gemignani, A., Ghelarducci, B., Varanini, M., 2004. Deriving the respiratory sinus arrhythmia from the heartbeat time series using empirical mode decomposition. In: Proc., Towards a New Vision of Complexity. Elsevier Ltd, pp. 171–177.
Barner, K.E., Weng, B., 2008. Optimal signal reconstruction using the empirical mode decomposition. Eurasip J. Adv. Signal Process. 12.
Althouse, B.M., Ng, Y.Y., Cummings, D.A., 2011). Prediction of dengue incidence using search query surveillance. PLoS neglected tropical diseases 5 (8).
Bieda, M.S., Lesiak, P., Woliski, T.R., Semenova, Y., Farrell, G., 2015. Demodulation algorithm using the Hilbert transform for a dynamic polarimetric optical fiber sensor. IEEE Sensors J. 15 (11), 6664–6670.
Boche, H., Monich, U.J., 2012. Extension of the Hilbert transform. In: Proc., 2012 IEEE International Conference on Acoustics, Speech, and Signal Processing, ICASSP 2012, March 25–March 30. Institute of Electrical and Electronics Engineers Inc, pp. 3697–3700.
Cao, Z., Lu, G., 2015. Research of the application of the Fourier transform algorithm for parabolic equation in radio wave diffraction. In: Proc., 7th Asia-Pacific Conference on Environmental Electromagnetics, CEEM 2015, November 4–November 7. Institute of Electrical and Electronics Engineers Inc, pp. 94–96.
Chao, C.-J., Tsai, S.-C., Lee, C.-H., Wang, T.-H., Lin, H.-C.K., 2014. The impact of affective tutoring system and information literacy on elementary school students' cognitive load and learning outcomes. In: Proc., 22nd International Conference on Computers in Education, ICCE 2014, November 30–December 4. Asia-Pacific Society for Computers in Education, pp. 847–856.
Chaudhury, K.N., Unser, M., 2011. On the Hilbert transform of wavelets. IEEE Trans. Signal Process. 59 (4), 1890–1894.
Chen, S.-C., Hsieh, M.-H., 2012. Modeling the transmission dynamics of dengue fever: implications of temperature effects. Sci. Total Environ. 431, 385–391.
Chen, S.-C., Liao, C.-M., Chio, C.-P., Chou, H.-H., You, S.-H., Cheng, Y.-H., 2010a. Lagged temperature effect with mosquito transmission potential explains dengue variability in southern Taiwan: insights from a statistical analysis. Sci. Total Environ. 408 (19), 4069–4075.
Chen, X., Wu, Z., Huang, N.E., 2010b. The time-dependent intrinsic correlation based on the empirical mode decomposition. Adv. Adapt. Data Anal. 2 (02), 233–265.
Chien, L.-C., Yu, H.-L., 2014. Impact of meteorological factors on the spatiotemporal patterns of dengue fever incidence. Environ. Int. 73, 46–56.
Chiu, C.-H., Wen, T.-H., Chien, L.-C., Yu, H.-L., 2014. A probabilistic spatial dengue fever risk assessment by a threshold-based-quantile regression method. PLoS One 9 (10), e106334.
Cho, S.-H., Jang, G., Kwon, S.-H., 2010. Time-frequency analysis of power-quality disturbances via the Gabor-Wigner transform. IEEE Trans. Power Deliv. 25 (1), 494–499.
Christophers, S., 1960. Aedes aegypti (L.) the yellow fever mosquito: its life history, bionomics and structure. In: Aëdes Aegypti (L.) the Yellow Fever Mosquito: Its Life History, Bionomics and Structure.
Daubechies, I., 1990. The wavelet transform, time-frequency localization and signal analysis. IEEE Trans. Inf. Theory 36 (5), 961–1005.
Deprem, Z., Cetin, A.E., 2015. Kernel estimation for time-frequency distribution [Zaman-Frekans Dailimi Icin Cekirdek Kestirimi]. In: Proc., 2015 23rd Signal Processing and Communications Applications Conference, SIU 2015, May 16–May 19. Institute of Electrical and Electronics Engineers Inc, pp. 1973–1976.
Diaz, M., Esteller, R., 2007. Comparison of the non linear energy operator and the Hilbert transform in the estimation of the instantaneous amplitude and frequency [Comparacion del operador de energia no lineal y la transformada de Hilbert en la estimacion de la amplitud y frecuencia instantaneas]. IEEE Lat. Am. Trans. 5 (1), 1–8.
Du, X.-L., He, L.-Z., 2009. New method of processing the boundary problem in the empirical mode decomposition (EMD). Beijing Gongye Daxue Xuebao 35 (5), 626–632.
Ebi, K.L., Nealon, J., 2016. Dengue in a changing climate. Environ. Res. 151, 115–123.
Endo, D., Hiyane, T., Atsuta, K., Kondo, S., 1998. Fractal image compression by the classification in the wavelet transform domain. In: Proc., Proceedings of the 1998 International Conference on Image Processing, ICIP. Part 2 (of 3), October 4–October 7. IEEE Comp Soc, pp. 788–792.
Fisman, D.N., Tuite, A.R., Brown, K.A., 2016. Impact of El Niño southern oscillation on infectious disease hospitalization risk in the United States. Proc. Natl. Acad. Sci. 113 (51), 14589–14594.
Flandrin, P., Rilling, G., Goncalves, P., 2004. Empirical mode decomposition as a filter bank. IEEE signal processing letters 11 (2), 112–114.
Fukushima, T., Hara-Yamamura, H., Urai, M., Kasuga, I., Kurisu, F., Miyoshi, T., Kimura, K., Watanabe, Y., Okabe, S., 2014. Toxicity assessment of chlorinated wastewater effluents by using transcriptome-based bioassays and Fourier transform mass spectrometry (FT-MS) analysis. Water Res. 52, 73–82.
Gabor, D., 1946. Theory of communication. Part 1: the analysis of information. J. Inst. Electr. Eng. 93 (26), 429–441.
Haar, A., 1910. Zur Theorie der orthogonalen Funktionensysteme. Math. Ann. 69 (3), 331–371.
Han, J., Wang, Q., Qin, K., 2013. The non-stationary signal of time-frequency analysis based on fractional Fourier transform and Wigner-Hough transform. In: Proc., 2013 International Conference on Mechatronics and Automatic Control Systems, ICMS 2013, August 10–August 11. Springer Verlag, pp. 1047–1054.
Hanus, R., 2015. Application of the Hilbert transform to measurements of liquid-gas flow using gamma ray densitometry. Int. J. Multiphase Flow 72, 210–217.
Heisenberg, W., 1927. Über den anschaulichen Inhalt der quantentheoretischen Kinematik und Mechanik. Z. Phys. 43 (3–4), 172–198.
Hory, C., Mellet, C., Valiere, J.C., Depollier, C., 2001. Local polynomial-time-frequency transform formulation of the pseudo-L-Wigner distribution. Signal Process. 81 (1), 233–237.
Hu, G., Li, R., Zheng, J., Tao, L., 2015. Power quality disturbance based on Gabor-Wigner transform. J. Inf. Comput. Sci. 12 (1), 329–337.
Huang, Y., Schmitt, F.G., 2014. Time dependent intrinsic correlation analysis of

temperature and dissolved oxygen time series using empirical mode decomposition. J. Mar. Syst. 130, 90–100.
Huang, N.E., Shen, Z., Long, S.R., Wu, M.C., Shih, H.H., Zheng, Q., Yen, N.-C., Tung, C.C., Liu, H.H., 1998. The empirical mode decomposition and the Hilbert spectrum for nonlinear and non-stationary time series analysis. Proc. R. Soc. Lond. A 454 (1971), 903–995.
Hudspeth, R.T., Medina, J.R., 1988. Wave group analysis by the Hilbert transform. In: Proc., Twenty-First Coastal Engineering Conference, June 20–June 25. Publ by ASCE, pp. 884–898.
Jing, N., Jiegang, P., 2009. Repression of the cross-term interference based on EMD and Cohen's class distribution. In: Proc., 2009 IEEE Circuits and Systems International Conference on Testing and Diagnosis, ICTD'09, April 28–April 29. IEEE Computer Society, Institute of Electrical and Electronics Engineers, IEEE; IEEE Circuits and Systems Society, CASS.
Kolivras, K.N., 2010. Changes in dengue risk potential in Hawaii, USA, due to climate variability and change. Clim. Res. 42 (1), 1–11.
Li, E.Y., Tung, C.-Y., Chang, S.-H., 2016. The wisdom of crowds in action: forecasting epidemic diseases with a web-based prediction market system. Int. J. Med. Inform. 92, 35–43.
Liao, C.-M., Huang, T.-L., Lin, Y.-J., You, S.-H., Cheng, Y.-H., Hsieh, N.-H., Chen, W.-Y., 2014. Regional response of dengue fever epidemics to interannual variation and related climate variability. Stoch. Env. Res. Risk A. 29 (3), 947–958.
Liu, R., 2015. Analysis of the interference modulation depth in the Fourier transform spectrometer. Adv. OptoElectron. 2015.
Liu, M., Kou, K.I., Morais, J., Dang, P., 2015. Signal moments for the short-time Fourier transform associated with hardy-Sobolev derivatives. Math. Meth. Appl. Sci. 38 (13), 2719–2730.
Liu, J., Liu, Z., Qi, Y., Peng, J., Sun, X., 2016. Prediction of deep-water reservoir by seiemic frequency division technology. Shiyou Xuebao/Acta Petrolei Sinica 37 (1), 80–87.
Mansour, Y., Sahar, S., 2000. Implementation issues in the Fourier transform algorithm. Mach. Learn. 40 (1), 5–33.
Maria de Medeiros, V., César Ugulino Araújo, M., Kawakami Harrop Galvão, R., Cirino da Silva, E., Cristina Bezerra Saldanha, T., Antonieta Salata Toscano, I., do Socorro Ribeiro de Oliveira, M., Kêlia Barbosa Freitas, S., Mariano Neto, M., 2005. Screening analysis of river seston downstream of an effluent discharge point using near-infrared reflectance spectrometry and wavelet-based spectral region selection. Water Res. 39 (13), 3089–3097.
Mesfioui, R., Love, N.G., Bronk, D.A., Mulholland, M.R., Hatcher, P.G., 2012. Reactivity and chemical characterization of effluent organic nitrogen from wastewater treatment plants determined by Fourier transform ion cyclotron resonance mass spectrometry. Water Res. 46 (3), 622–634.
Meyer, Y., 1991. Ondelettes et opérateurs. Hermann 3 (2), 253–264.
Morlet, J., Arens, G., Fourgeau, E., Glard, D., 1982. Wave propagation and sampling theory—part I: complex signal and scattering in multilayered media. Geophysics 47 (2), 203–221.
Oberlin, T., Meignen, S., Perrier, V., 2012. An alternative formulation for the empirical mode decomposition. IEEE Trans. Signal Process. 60 (5), 2236–2246.
Okumura, S., 2011. The Short Time Fourier Transform and Local Signals. ProQuest LLC.
O'Neill, J.C., Williams, W.J., 1998. Distributions in the discrete Cohen's classes. In: Proc., 1998 23rd IEEE International Conference on Acoustics, Speech and Signal Processing, ICASSP 1998, May 12–May 15. Institute of Electrical and Electronics Engineers Inc, pp. 1581–1584.
Papadimitriou, S., Sun, J., Philip, S.Y., 2006. Local correlation tracking in time series. In: Data Mining, 2006. ICDM'06. Sixth International Conference on. IEEE, pp. 456–465 December.
Park, D., Roesner, L.A., 2012. Evaluation of pollutant loads from stormwater BMPs to receiving water using load frequency curves with uncertainty analysis. Water Res. 46 (20), 6881–6890.
Rabinovitch, I., Venetsanopoulos, A.N., 1997. High quality image compression using the wavelet transform. In: Proc., Proceedings of the 1997 International Conference on Image Processing. Part 2 (of 3), October 26–October 29. IEEE Comp Soc, pp. 283–286.
Rao, A.R., Hsu, E.-C., 2008. Hilbert-Huang Transform Analysis of Hydrological and Environmental Time Series. Springer 2008 edition (March 4, 2008).
Reuben, S., Banas, K., Banas, A., Swarup, S., 2014. Combination of synchrotron radiation-based Fourier transforms infrared microspectroscopy and confocal laser scanning microscopy to understand spatial heterogeneity in aquatic multispecies biofilms. Water Res. 64, 123–133.
Schuchardt, P., Siesler, H.W., 2016. Real-time analysis of the polymerization kinetics of 1,4-butanediol and 4,4-diphenylmethanediisocyanate by fiber-coupled Fourier transform infrared spectroscopy. Anal. Bioanal. Chem. 1–7.
Skublewska-Paszkowska, M., Smolka, J., 2008. The influence of picture quality scale measure on choosing the wavelet transform during image compression. In: Proc., International Conference on Computer Vision and Graphics, ICCVG 2008, November 10–November 12. Springer Verlag, pp. 70–79.
Song, L.-X., Wang, Q., Wang, Y.-J., Liang, K., 2007. Empirical mode decomposition method with intermittency test and separation. Harbin Gongcheng Daxue Xuebao 28 (2), 178–182.
Stankovic, L., Alieva, T., Bastiaans, M.J., 2003. Time-frequency signal analysis based on the windowed fractional Fourier transform. Signal Process. 83 (11), 2459–2468.
Suen, Y., Xiao, S., Xiong, Y., Hao, S., Zhao, X., 2015. Time-frequency analysis system based on temporal Fourier transform. In: Proc., IEEE International Conference on Communication Problem-Solving, ICCP 2015, October 16–October 18. Institute of Electrical and Electronics Engineers Inc, pp. 97–100.
Suriyawichitseranee, A., Grigoriev, Y.N., Meleshko, S.V., 2015. Group analysis of the Fourier transform of the spatially homogeneous and isotropic Boltzmann equation with a source term. Commun. Nonlinear Sci. Numer. Simul. 20 (3), 719–730.
Titchmarsh, E.C., 1948. Introduction to the Theory of Fourier Integrals. Oxford University Press.
Torrence, C., Compo, G.P., 1998. A practical guide to wavelet analysis. Bull. Am. Meteorol. Soc. 79 (1), 61–78.
Tseng, W.-C., Chen, C.-C., Chang, C.-C., Chu, Y.-H., 2009. Estimating the economic impacts of climate change on infectious diseases: a case study on dengue fever in Taiwan. Clim. Chang. 92 (1–2), 123–140.
Tung, Y.-T., Wu, M.-F., Wang, G.-J., Hsieh, S.-L., 2014. Nanostructured electrochemical biosensor for th0065 detection of the weak binding between the dengue virus and the CLEC5A receptor. Nanomedicine 10 (6), 1335–1341.
Valtierra-Rodriguez, M., Romero-Troncoso, R.J., Garcia-Perez, A., Osornio-Rios, R.A., 2013. FPGA-based instantaneous estimation of unbalance/symmetrical components through the Hilbert transform. In: Proc., 39th Annual Conference of the IEEE Industrial Electronics Society, IECON 2013, November 10–November 14. IEEE Computer Society, pp. 2279–2284.
Van Panhuis, W.G., Choisy, M., Xiong, X., Chok, N.S., Akarasewi, P., Iamsirithaworn, S., ... Vongphrachanh, P., 2015. Region-wide synchrony and traveling waves of dengue across eight countries in Southeast Asia. Proc. Natl. Acad. Sci. 112 (42), 13069–13074.
Wei, J.-H., Feng, C.-L., 2015. Fault feature extraction method based on SVD and optimal Morlet wavelet. Binggong Xuebao 36, 215–219.
Wigner, E., 1932. On the quantum correction for thermodynamic equilibrium. Phys. Rev. 40 (5), 749–759.
Wu, Z., Huang, N.E., 2009. Ensemble empirical mode decomposition: a noise-assisted data analysis method. Adv. Adapt. Data Anal. 1 (01), 1–41.
Wu, Z., Huang, N.E., 2010. On the filtering properties of the empirical mode decomposition. Adv. Adapt. Data Anal. 2 (4), 397–414.
Wu, P.-C., Lay, J.-G., Guo, H.-R., Lin, C.-Y., Lung, S.-C., Su, H.-J., 2009. Higher temperature and urbanization affect the spatial patterns of dengue fever transmission in subtropical Taiwan. Sci. Total Environ. 407 (7), 2224–2233.
Wu, J., Huang, R., Wan, J., Chen, Y., Yin, Y., Chen, G., 2016. Phase identification for space charge measurement under periodic stress of an arbitrary waveform based on the Hilbert transform. Meas. Sci. Technol. 27 (4).
Xu, X., Liu, X., Li, X., Xin, Q., Chen, Y., Shi, Q., Ai, B., 2016. Global snow cover estimation with microwave brightness temperature measurements and one-class in situ observations. Remote Sens. Environ. 182, 227–251.
Yang, C.-H., Hua, H., Tan, W., Iwai, K., Miyagi, M., Chi, N., Shi, Y.-W., 2010. Loss spectrum measurement for infrared hollow fiber based on the Fourier transform infrared spectrometer. Appl. Opt. 49 (13), 2504–2509.
Yen, N.c., 1994. Wave packet decomposition. J. Acoust. Soc. Am. 95 (2), 889–896.
Yu, H.-L., Yang, S.-J., Yen, H.-J., Christakos, G., 2011. A spatio-temporal climate-based model of early dengue fever warning in southern Taiwan. Stoch. Env. Res. Risk A. 25 (4), 485–494.
Zhang, L., Wang, S., Xu, Y., Shi, Q., Zhao, H., Jiang, B., Yang, J., 2016. Molecular characterization of lake sediment WEON by Fourier transform ion cyclotron resonance mass spectrometry and its environmental implications. Water research 106, 196–203.